INTERNATIONAL JOURNAL OF HEAT AND TECHNOLOGY

ISSN: 0392-8764
Vol. 35, No. 1, March 2017, pp. 53-58
DOI: 10.18280/ijht.350107

A publication of IIETA

IIETA International Information and Engineering Technology Association
Advancing the World of Information and Engineering

http://www.iieta.org/Journals/IJHT

Effect of heat treatment temperature on the structure and tribological properties of nanometer lanthanum borate

Yue Wang[1], Daikuan Huang[2*]

[1]School of Mechanical Engineering, Guizhou University, Guiyang, 550025, China
[2]Guizhou Academy of Environmental Sciences, Guiyang, 550025, China

Email: huangdaikuan@pku.edu.cn

ABSTRACT

Nanometer lanthanum borate was prepared by ultrasonic-assisted chemical precipitation. X-ray diffraction and a laser particle size analyzer were used to study the heat treatment temperature on the micro-structure of the nanoparticles, and the tribological properties of nanoparticles were explored for friction and wear using a MMU-10G testing machine. The results show that the heat treatment temperature not only determines the crystallization degree and crystal type of nanometer lanthanum borate, but also greatly affects the anti-friction and wear-resistance properties of the base oil. When the heat treatment temperature is between 300°C and 600°C, amorphous $La_2[B_4O_5(OH)_4]_3$ nanoparticles are formed. Featuring strong chemical activity, adsorption on the friction surface, and a significant anti-wear self-repair effect, the nanoparticles can promote the formation of a tribochemical reaction film. When the heat treatment temperature exceeds 900°C, the particle size distribution in the bed becomes broader and shifts to a larger size. Hard-phase crystal $LaBO_3$ and B_2O_3 particles are formed, which intensifies the abrasive wear and the tribological properties are reduced.

Keywords: Nanometer Lanthanum Borate, Heat Treatment, High Temperature Phase Change, Friction and Wear, Anti-Friction and Anti-Wear Mechanism.

1. INTRODUCTION

With the development of modern science and technology, the study and development of high-temperature tribology has become an important frontier of tribology [1]. However, tribology scholars are baffled by the problem of continuous lubrication from room temperature to high temperature. A possible solution to this problem lies in the improvement of the physical and chemical properties of nanomaterials via proper heat treatment. As a common choice for gear lubrication, borate is a type of highly efficient green lubricant additive which possesses pretty good thermal stability, excellent anti-wear properties under extreme pressure, and seal compatibility [2-4]. After heat treatment, the specific surface area and chemical activity of borate will increase due to the ensuing dehydration reaction; the physical and chemical properties will also change because a phase transition will occur in borate crystals under high temperature [5-7]. The changes will have an influence on the tribological properties of borate as a lubricant additive [8-10].

This paper studies the influence of heat treatment temperature on the tribological properties of nanometer lanthanum borate particles with a 45 steel-HT200 friction pair. The purpose of this study is to clarify the correspondence between the structure and performance of nanometer lanthanum borate, discuss the mode of action, identify the optimal heat treatment temperature, and thereby provide a technical basis for the further improvement of the application of nanometer lanthanum borate in lubrication technology.

2. EXPERIMENT

2.1 Test materials and heat treatment

The following materials were prepared for the tests: lanthanum nitrate $La(NO_3)_3.6H_2O$ (A.R.) (Tianjin Fine Chemical Institute); borax Na_2 $[B_4O_5(OH)_4]_3.8H_2O$) (A.R.) (Tianjin Hengxing Chemical Reagent Co., Ltd.); silane coupling agent KH550 (Shenzhen Chengqixin Technology Co., Ltd.); test oil (150N base oil).

The nanometer lanthanum borate was prepared by chemical precipitation and was ultrasonic-assisted; The details of the experiment are introduced in the 11th reference [11]. The reaction is shown in Formula (1).

$$2La(NO_3)_3.6H_2O + 3Na_2B_4O_5(OH)_4.8H_2O = La_2\left[B_4O_5(OH)_4\right]_3 \downarrow +6NaNO_3 + 36H_2O \quad (1)$$

The prepared nanometer lanthanum borate was placed in a muffle furnace to receive heat treatment for 5h at the temperatures of 300°C, 600°C, and 900°C, respectively. The morphological characteristics and phases of the heat treatment products were analyzed by a transmission electron microscope and an X-ray spectroscope. The surfaces of the prepared products were modified by the ethanol solution KH550 silane coupling agent, aiming at ensuring the good dispersion stability of the nanometer lanthanum borate particles in the base oil. The modified particles were dispersed into the base oil, stirred magnetically for 30min, and dispersed in an ultrasonic disperser for 30min. The oil samples were prepared as above, as this features stable suspension in the long term. Table 1 lists the codes for lubricant oil samples and friction samples.

Table 1. Codes for lubricant oil samples and friction samples

Heat treatment temperature	Oil samples	Friction samples
Original	AO (Base Oil)	HAO
300°C	BO	HBO
900°C	CO	HCO

2.2 Tribological tests

The tribological performance tests were carried out on an MMU-10G high-speed high-temperature friction and wear testing machine. The structure, size, and working position of the friction pair samples are described in Figure 1. The upper sample of the friction pair was made of 45hardened and tempered steel, while the lower sample was made of HT200. The surface roughness of the friction pairs was Ra0.8μm. Figure 1 consists of the 3D assembly drawing and the working diagram of the upper and lower samples. The tests were conducted in the following conditions: test load 200N (0.8MPa), rotating speed 419r/min (linear speed 0.5m/s), test time 40h, and average oil temperature 50-55 °C. The lubricant dispersion system in the friction and wear experiment was in the full infiltration state. The experiment lasted 40h, during which the equipment was stopped every 5h to unload, clean, and dry the friction samples. The dried samples were weighed with an electronic balance. The weight loss of each sample was recorded to establish the weight-loss time curve. The torque sensor of the testing equipment automatically collected the real-time friction coefficient per second. Based on the data, the author calculated the average friction coefficient within 5h, and established the average friction-coefficient time curve. The wear morphology and surface composition of the lower specimen were analyzed by scanning electron microscopy, atomic force microscopy, and an energy dispersive spectroscopy. Each test result is the average of that of three parallel tests.

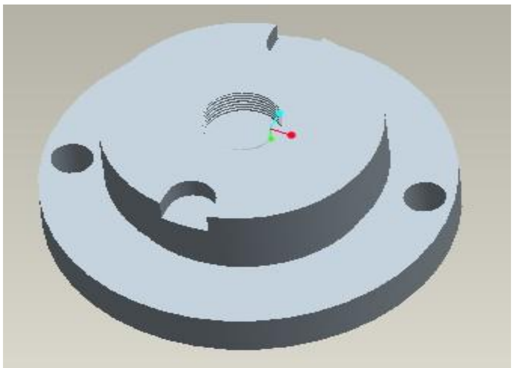

(a) Assembly drawing (3D)

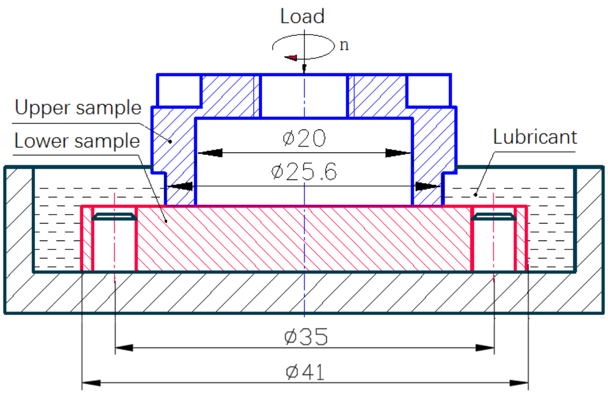

(b) Working diagram

Figure 1. Upper and lower samples of the friction pair

3. RESULTS AND DISCUSSION

3.1 Characterization of heat treatment products of nanometer lanthanum borate

The XRD patterns of the heat treatment products of nanometer lanthanum borate are displayed in Figure 2.

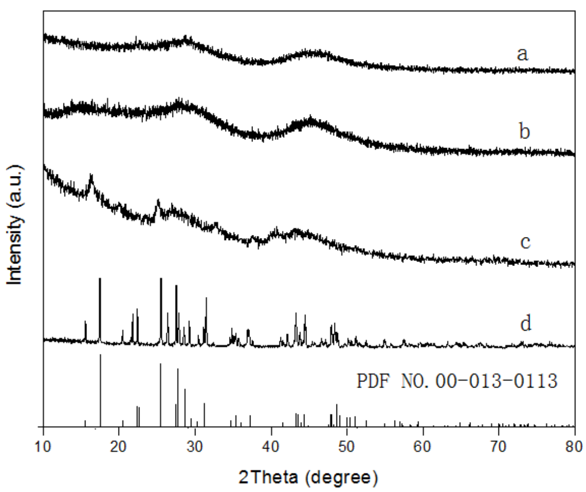

Figure 2. XRD patterns of the heat treatment products under different temperatures (a)Original lanthanum borate (b) 300°C (c) 600°C (d) 900°C

2(a) is the XRD spectral line of the original particles, and 2(b) is the XRD spectral line of particles treated under 300°C. Both spectral lines are wide and diffused gentle slopes without characteristic peaks, indicating that the nanometer lanthanum borate prepared in the corresponding temperature range is amorphous. With the increase of the treatment temperature, the intensity of the diffraction intensity of the samples gradually rises and sharp peaks start to emerge at 600°C (2(c)). 2(d) is the XRD spectral line of the sample obtained after calcinating lanthanum borate at 900°C. Its diffraction peak coincides with the standard spectrum of lanthanum borate on the PDF.No.00-013-0113 card. This means $LaBO_3$, nanometer lanthanum borate, is an orthogonal crystal (lattice parameters: a = 0.5104nm, b = 0.8252nm, c = 0.5872nm) when the temperature reaches 900°C. According to the above results, when the calcination temperature rises to 900°C, the amorphous $La_2[B_4O_5(OH)_4]_3$ undergoes a transition to well-crystallized orthorhombic $LaBO_3$ (phase transition). Meanwhile, Table 2 shows the grain size also expands rapidly. The equation of the calcination and decomposition of nanometer lanthanum borate is shown in Formula (2).

$$La_2[B_4O_5(OH)_4]_3 = La_2BO_3 + 5B_2O_5 + 6H_2O \quad (2)$$

where B_2O_3 is mostly amorphous [12,13].

Table 2. Particle sizes of the heat treatment products under different temperatures

Heat treatment temperature	D10/nm	D50/nm	D97/nm
300°C	10	30	80
900°C	35	140	550

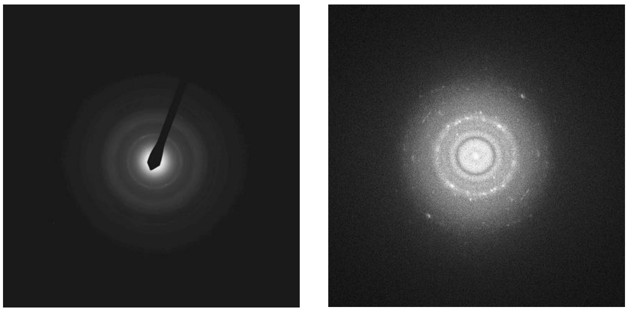

(a) Original (b) Heat-treated (900°C)

Figure 3. Electron diffraction patterns of lanthanum borate

Figures 3(a) and 3(b) show the electron diffraction patterns of the two products before and after the heat treatment of lanthanum borate. As shown in Figure 3(a), there is almost no visible diffraction ring for the original lanthanum borate except for some faint, dispersed concentric rings. By contrast, Figure 3(b) carries bright and clear diffraction rings that have resulted from single-crystal face diffraction. The comparison reveals that the prepared $La_2[B_4O_5(OH)_4]_3$ nanoparticles are amorphous [14], and are transformed into the crystal $LaBO_3$ through calcination under 900°C [15].

The above transformation process of nanometer lanthanum borate can be summarized as follows: At below 600°C, the interbedded water and a small amount of absorbed water are removed, and the amorphous structure is not changed; when the temperature reaches 600°C, the $La_2[B_4O_5(OH)_4]_3$ nanoparticles start to lose hydroxide radicals and a small amount of new-phase B_2O_3 comes into being. At 900°C and above, the products are transformed into well-crystallized orthorhombic $LaBO_3$.

3.2 Tribological properties

3.2.1 Anti-wear properties

Figure 4 presents the results of the wear-induced weight-loss tests. The nanometer lanthanum borate containing samples was tested under three oil sample lubrication conditions: the base oil, 300°C heat treatment, and 900°C heat treatment. As can be seen from Figure 4, the wear-induced weight losses of the HAO and HCO samples almost increase monotonically. The two samples change in a similar trend. The weight losses are significant in the initial period, and tend to ease in the middle and later periods. The weight loss of HBO is much smaller than that of HAO and HCO. The wear is obvious initially, but turns negative shortly afterwards. Table 3 lists the total wear-induced weight losses of the three samples. The total weight losses of the friction pair under the three oil sample lubrication conditions are ranked as: HAO>HCO>HBO>0, indicating that the total wears of the three lubricants are all positive but of different degrees. HBO has the least weight loss at 0.7 mg, which is 45 % lower than that of HCO and 66 % lower than that of HAO.

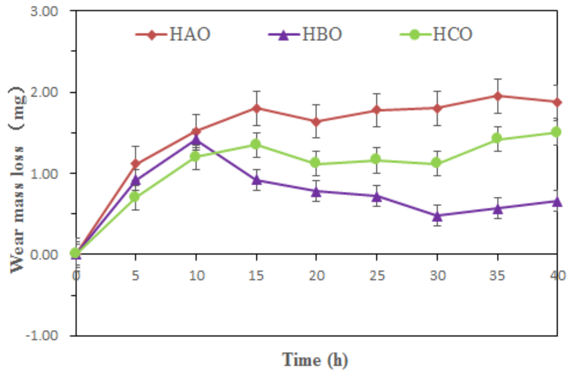

Figure 4. Relationship between wear-induced loss and time of each sample

Table 3. Wear-induced weight loss of the lower sample of the friction pair

Friction sample	HAO	HBO	HCO
Weight loss of the lower sample	1.98	0.70	1.27

3.2.2 Anti-friction performance

Figure 5 shows the relation curve between the friction coefficient and the test time.

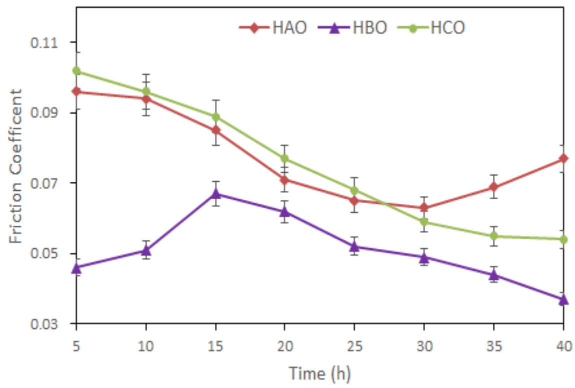

Figure 5. Friction-coefficient time curves of different lubrication systems

From 0h to 25h, the AO oil sample and CO oil sample have similar friction coefficients; after 25h, the anti-friction performance of the CO oil sample is much better than that of the AO oil sample. The comparison demonstrates that it is not until the later period that $LaBO_3$ nanoparticles have friction resistance. In addition, the similarity of the two samples in terms of the average friction coefficient shows that the $LaBO_3$ nanoparticles formed by heat treatment under 900°C have a similar friction reduction effect with the base oil. It is also revealed in the figure that the BO oil sample has a significantly lower friction coefficient than AO (base oil) oil sample and CO oil sample throughout the entire process. This proves that the amorphous $La_2[B_4O_5(OH)_4]_3$ nanoparticles can significantly improve the anti-friction performance of base oil, thus achieving a better anti-friction effect than the crystal nanoparticles of $LaBO_3$. The BO oil sample reduces the average friction coefficient of the base oil sample by 35 %.

3.3 Friction surface morphology and elementary composition

Figure 6 illustrates the SEM morphology of wear scars on the lower sample after the friction pair has run for 40h.

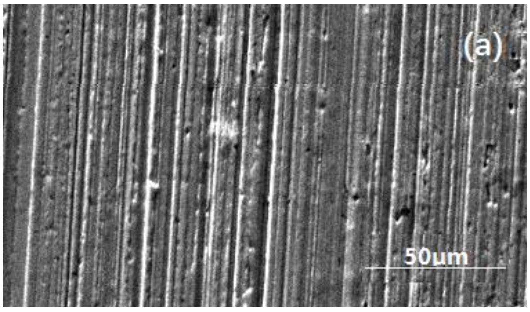

(a) HAO

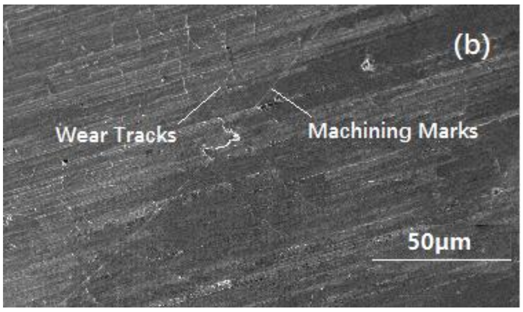

(b) HBO

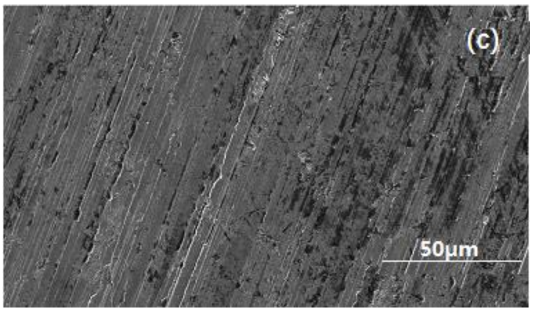

(c) HCO

Figure 6. SEM patterns of the worn surfaces after the friction pair has run for 40h

As shown in Figure 6(a), the sample HAO has wider and deeper surface scratches than other samples. The scratches feature sharp edges and clear grooves, in which there is no deposition of foreign matter. In Figure 6(b), a continuous stretch of a light gray recovered layer is formed on the surface of sample HBO, which fills up the friction scratches. Thus, the scratches become shallow and smooth on the surface. This indicates that the sedimentary layer has excellent wear compensation, making the sample the least worn among all samples. According to Figure 6(c), there are dark spots on the surface of sample HCO; the grooves are thin, narrow, and full of linear dark color sediments. The precipitation of foreign matter compensates for the wear-induced loss to a limited extent.

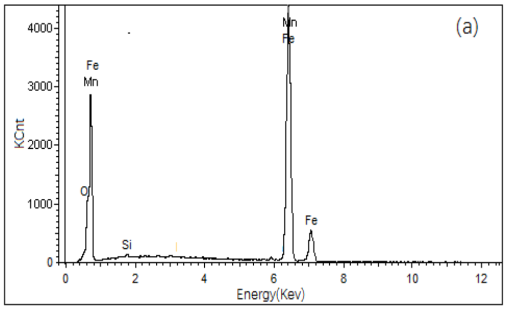

(a) HAO

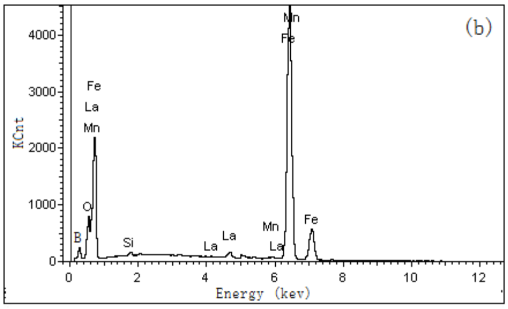

(b) HBO

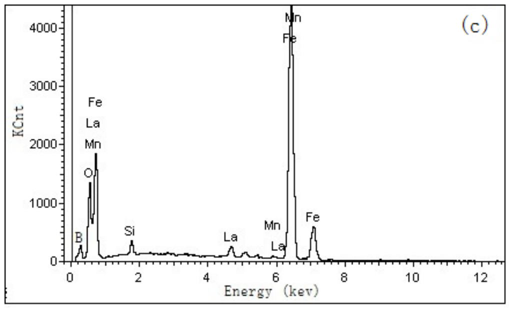

(c) HCO

Figure 7. Results of EDS analysis of friction surfaces

Table 4. Comparison between atomic contents of main elements of the friction surfaces (At%)

Element	Fe K	Mn K	Si K	O K	La K	B K
HAO	98.75	0.36	0. 38	0.51	0.00	0.00
HBO	83.20	0.61	0. 75	9.19	2.19	8.14
HCO	73.06	0.58	0.44	9.26	5.01	11.65

Figure 7 and Table 4 show the EDS analysis results of the surface elements of HAO, HBO, and HCO. It can be inferred from the table that La, B, and O, the characteristic elements on the surfaces of samples HBO and HCO, have permeated to the surface and sub-surface layers of the friction surfaces of the samples. In other words, the nanoparticles have been involved in the complex reactions to form the self-repair layers on the friction surfaces. According to Table 4, HCO contains a higher percentage of La, B, and O, the characteristic elements of the self-repair film layer on the friction surface, than HBO. Thus, HCO is less capable of self-repairing than HBO. The main reason is that the crystal $LaBO_3$ does not contain hydroxide radicals. As the surface is less likely to be activated under high temperatures, the sample contributes less to the precipitation of the repair layer than the amorphous $La_2[B_4O_5(OH)_4]_3$. The crystal $LaBO_3$, i.e. the product of the heat treatment under 900°C, contains a small amount of hard-phase material B_2O_3. The sample surface is worn more severely due to the abrasive wear of hard particles, leading to the formation of new grooves. As a result, the surface roughness decreases, the surface energy declines, and thus the friction resistance grows.

3.4 Discussion of the anti-friction and anti-wear mechanism

In light of the analysis of the test results, the author has obtained the following findings: In the molecular structure of the amorphous nanometer lanthanum borate, the boron-oxygen backbones of $[B_4O_5(OH)_4]^{2-}$ are linked up to form a chain system of hydrogen bonds [16] (Figure 9). The structural instability of the hydrogen bonds under high temperatures causes the breaking of chemical bonds, the removal of hydroxyl radicals, and the release of a large amount of crystal water and reactive oxygen. The resulting expansion of the specific surface area and increase in chemical activity of the nanometer lanthanum borate [17-19], on the one hand, activate the catalytic performance of the rare-earth element La, resulting in the boronization between the B and Fe base [11], the formation of FeB film (low-binding energy), and the effective reduction in contact force and abrasive wear [20]. On the other hand, they help with the formation of an La_2O_3 oxidation film between La and reactive oxygen, which compensates for the surface wear and thus reduces friction and wear.

In view of the previous research [21,22] and the test results of this paper, the author finds that the tribological properties of nanometer lanthanum borate can be greatly improved through thermal activation under 300°C-600°C because the formation of the composite repair film layer, which contains FeB and La_2O_3, further enhances the anti-friction and lubrication performance of heat-treated nanometer lanthanum borate. On the contrary, the nanometer lanthanum borate treated under 900°C produces B_2O_3, a hard, ceramic material, through a cracking reaction. The wear-induced loss is increased as hard-phase B_2O_3 and large-size $LaBO_3$ exacerbate the abrasive wear.

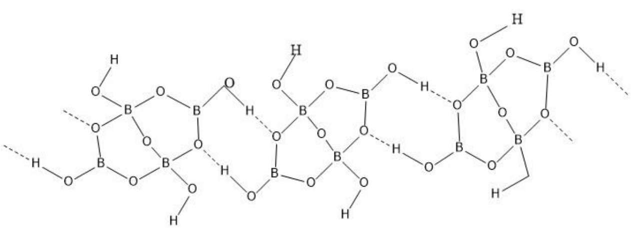

Figure 8. Chain structure of hydrogen bonds of $[B_4O_5(OH)_5]^{2-}$

4. CONCLUSIONS

After heat treatment, the nanometer lanthanum borate prepared by chemical precipitation undergoes a four-stage phase change process: At below 300°C, the absorbed water is lost; between 300° and 600°C, most crystal water and hydroxy water are removed; between 600° and 900°C, the remaining hydroxy water is gone; at 900°C, the particles are decomposed into crystal $LaBO_3$.

The amorphous $La_2[B_4O_5(OH)_4]_3$ nanoparticles obtained through moderate heat treatment under 300°C-600°C boast strong adsorption on the friction surface, and promote the complex boronization and formation of an oxidation film on the friction surface, thereby further improving the tribological performance of the lubricant additive nanometer lanthanum borate.

When the heat treatment surpasses 900°C, the nanoparticles are cracked to produce large-size $LaBO_3$ nanoparticles and hard-phase B_2O_3 particles, which together exacerbate abrasive wear and reduce the tribological properties.

$La_2[B_4O_5(OH)_4]_3$ nanoparticles show an excellent anti-friction and lubrication performance because the particles can form a self-repair film on the surface of the HT200 friction pair, which contains characteristic elements like Fe, B, La, and O, through a tribochemical reaction under the action of friction heat.

ACKNOWLEDGMENT

This work was supported by the Guizhou Foundation for Science and Technology (No.20122119)- the project of the preparation of multiphase nanometer materials, and its tribology performance in oil.

REFERENCES

[1] Stachowiak G., Batchelor A.W. (2013). *Engineering Tribology*, USA, Butterworth-Heinemann, pp. 128-136.

[2] Shahnazar S., Bagheri S., Hamid S.B.A. (2016). Enhancing lubricant properties by nanoparticle additives, *International Journal of Hydrogen Energy*, Vol. 41, No. 4, pp. 3153-3170. DOI: 10.1016/ j.ijhydene. 2015.12. 040

[3] Qiao Y.L., Xu B.S. (2005). *Lubrication and Self Repairing Technology of Nanoparticles*, National Defense Industry Press, Beijing, pp. 69-77.

[4] Gu K.C., Chen B.S., Chen Y. (2013). Preparation and tribological properties of lanthanum-doped TiO_2 nanoparticles in rapeseed oil, *Journal of Rare Earths*, Vol. 31, No. 6, pp. 589-594.

[5] Maier M., Trandafir D.L., Simon S. (2016). Effect of heat treatment time on local structure of lanthanum-aluminum–gallium-borate xerogels, *Ceramics International*, Vol. 42, No. 4, pp. 4764-4767.

[6] Turcu F.R., Samoson A., Maie M., Trandafir D.L., Simon S. (2016). High fraction of penta-coordinated aluminum and gallium in lanthanum–aluminum–gallium borates, *Journal of the American Ceramic Society*, Vol. 99, No. 8, pp. 2795-2800.

[7] Khanafer K., Vafai K.A. (2011). Critical synthesis of thermophysical characteristics of nanofluids, I*nternational Journal of Heat and Mass Transfer*, Vol. 54, No. 19, pp. 4410-4428.

[8] Qiu Y., Khonsari M.M. (2011). Experimental investigation of tribological performance of laser textured stainless steel rings, *Tribology International*, Vol. 44, No. 5, pp. 635-644. DOI: 10.1016/j.triboint.2011.01.003

[9] Franco M., Sha W., Aldic G., Çimenoğlu H. (2016). Effect of reinforcement and heat treatment on elevated temperature sliding of electroless Ni–P/SiC composite

coatings, *Tribology International*, Vol. 97, pp. 265-271. DOI: 10.1016/j.triboint.2016.01.047
[10] Mahmud T.B., Farrokhzad M.A., Khan T.I. (2017). Effect of heat treatment on wear performance of nanostructured WC-Ni/Cr HVOF sprayed coatings, *Tribology Online*, Vol. 12, No. 1, pp. 18-28. DOI: 10.2474/trol.12.18
[11] Wang Y., Zhou Y.K., Huang D.K. (2016). The tribology performance of $La_2[B_4O_5(OH)_4]_3$/in composite nanoparticles in rapeseed oil., *Non-Metallic Mines*, Vol. 39, No. 6, pp. 82-85.
[12] Tavoosi M., Ghasemi A., Yousefi D. (2016). Crystallization behavior, microstructure and magnetic properties of B_2O_3-SiO_2-Fe_2O_3-BaO-SrO glass-ceramics, *Journal of Ceramic Science and Technology*, Vol. 7, No. 4, pp. 469-475.
[13] Dub N., Brazhkin V.V., Belous V.A., Tolmacheva G.N., Konevskii P.V. (2014). Comparative nanoindentation of single crystals of hard and superhard oxidess, *Journal of Superhard Materials*, Vol. 36, No. 4, pp. 217-230. DOI: 10.3103/S1063457614040017
[14] Solozhenko V.L., Kurakevych O.O., Brazhkin V.V., Godec Y.L. (2015). Thermodynamically consistent p–t phase diagram of boron oxide B_2O_3 by in situ probing and thermodynamic analysis, *The Journal of Physical Chemistry C*, Vol. 119, No. 35, pp. 20600-20605.
[15] Wang W.H. (2013). The nature and characteristics of amorphous material, *Advances in Physics*, Vol. 33, No. 5, pp. 177-351.
[16] Gao R., Zhang Z.J., Zhao J.T. (2014). Research on the crystal structure and temperature (pressure) phase change of boric acid salt, *Journal of Chinese Rare Earths*, Vol. 32, No. 4, pp. 385-396.
[17] Gao Y., Zhao Y.Y., Di W.J. (2014). Research of new actinoid boric acid salt structure, *Journal of Nuclear and Radiochemistry*, Vol. 36, No. 1, pp. 1-16.
[18] Koshigan K.D., Panman M.R., Bakker B.H., Den U.D., Kay E.R., Leigh D.A., Buma W.J. (2013). Water lubricates hydrogen-bonded molecular machines, *Nature Chemistry*, Vol. 11, No. 5, pp. 929-934. DOI: 10.1038/nchem.1744 1719
[19] Koshigan K.D., Mangolini F., Mcclimon J.B., Vacher B., Bec S., Carpick R.W. (2015). Understanding the hydrogen and oxygen gas pressure dependence of the tribological properties of silicon oxide–doped hydrogenated amorphous carbon coatings, *Carbon*, Vol. 93, pp. 851-860.
[20] Cimenoglu H., Atar E., Motallebzadeh A. (2014). High temperature tribological behaviour of borided surfaces based on the phase structure of the boride layer, *Wear*, Vol. 309, No. 1, pp. 152-158. DOI: 10.1016 /j. wear.2013.10.012
[21] Wang J.T., Wen L.Y., Wang T., Wang Y.L., Gao Y.L. (2015). First-principles study on the thermodynamic defect and crystal structure of U-12.5 At% Nb alloy, *International Journal of Heat and Technology*, Vol. 33, No. 1, pp. 175-180. DOI: 10.18280/ijht.330124
[22] Wu S.T., Wu G.X. (2015). Preparation and characterization of Fe_2O_3 micro-nano materials, *International Journal of Heat and Technology*, Vol. 33, No. 2, pp. 57-62. DOI: 10.18280/ijht.330209